European Radiology (2022) 32:7365–7373
https://doi.org/10.1007/s00330-022-08772-w

MOLECULAR IMAGING

Breast cancer imaging with glucosamine CEST (chemical exchange saturation transfer) MRI: first human experience

Michal Rivlin[1] · Debbie Anaby[2,3] · Noam Nissan[2,3] · Moritz Zaiss[4] · Anagha Deshmane[5] · Gil Navon[1] · Miri Sklair-Levy[3,6]

Received: 26 November 2021 / Revised: 22 March 2022 / Accepted: 25 March 2022 / Published online: 14 April 2022

Abstract

Objectives This study aims to evaluate the feasibility of imaging breast cancer with glucosamine (GlcN) chemical exchange saturation transfer (CEST) MRI technique to distinguish between tumor and surrounding tissue, compared to the conventional MRI method.

Methods Twelve patients with newly diagnosed breast tumors (median age, 53 years) were recruited in this prospective IRB-approved study, between August 2019 and March 2020. Informed consent was obtained from all patients. All MRI measurements were performed on a 3-T clinical MRI scanner. For CEST imaging, a fat-suppressed 3D RF-spoiled gradient echo sequence with saturation pulse train was applied. CEST signals were quantified in the tumor and in the surrounding tissue based on magnetization transfer ratio asymmetry (MTRasym) and a multi-Gaussian fitting.

Results GlcN CEST MRI revealed higher signal intensities in the tumor tissue compared to the surrounding breast tissue (MTRasym effect of 8.12 ± 4.09%, $N = 12$, $p = 2.2$ E−03) with the incremental increase due to GlcN uptake of 3.41 ± 0.79% ($N = 12$, $p = 2.2$ E−03), which is in line with tumor location as demonstrated by T_1W and T_2W MRI. GlcN CEST spectra comprise distinct peaks corresponding to proton exchange between free water and hydroxyl and amide/amine groups, and relayed nuclear Overhauser enhancement (NOE) from aliphatic groups, all yielded larger CEST integrals in the tumor tissue after GlcN uptake by an averaged factor of 2.2 ± 1.2 ($p = 3.38$ E−03), 1.4 ± 0.4 ($p = 9.88$ E−03), and 1.6 ± 0.6 ($p = 2.09$ E−02), respectively.

Conclusion The results of this initial feasibility study indicate the potential of GlcN CEST MRI to diagnose breast cancer in a clinical setup.

Key Points

- *GlcN CEST MRI method is demonstrated for its the ability to differentiate between breast tumor lesions and the surrounding tissue, based on the differential accumulation of the GlcN in the tumors.*
- *GlcN CEST imaging may be used to identify metabolic active malignant breast tumors without using a Gd contrast agent.*
- *The GlcN CEST MRI method may be considered for use in a clinical setup for breast cancer detection and should be tested as a complementary method to conventional clinical MRI methods.*

Keywords Magnetic resonance imaging · Glucosamine · Breast neoplasms · Diagnostic imaging · Contrast media

Michal Rivlin and Debbie Anaby contributed equally to this work.

✉ Gil Navon
navon@tauex.tau.ac.il

[1] School of Chemistry, Tel-Aviv University, Levanon St., 6997801 Tel Aviv, Israel

[2] Department of Radiology, Sheba Medical Center, Sheba Tel Ha'shomer, Emek Ha Ella 1 St, 5265601 Ramat-Gan, Israel

[3] The Sackler School of Medicine, Tel-Aviv University, Levanon St., 6997801 Tel Aviv, Israel

[4] Departmnet of Neuroradiology, University Clinic Erlangen, Friedrich-Alexander Universität Erlangen-Nürnberg (FAU), Erlangen, Germany

[5] Department of Biomedical Magnetic Resonance, University of Tübingen, Tübingen, Germany

[6] Meirav High Risk Clinic, Department of Diagnostic Imaging, Sheba Medical Center, Emek Ha Ella 1 St, 5265601 Ramat Gan, Israel

Abbreviations

CEST	Chemical exchange saturation transfer
Gd	Gadolinium
GlcN	Glucosamine
MRI	Magnetic resonance imaging
MT	Magnetization transfer
MTRasym	Magnetization transfer ratio asymmetry
NOE	Nuclear Overhauser enhancement
ROI	Region of interest
T_1W	T_1-weighted
T_2W	T_2-weighted

Introduction

Chemical exchange saturation transfer (CEST) MRI enables to obtain images of endogenous cellular components or exogenous agents that contain exchangeable protons. CEST effects are detected indirectly through the reduction of the water signal following selective saturation of exchangeable protons on the CEST agent [1] (for reviews, see, e.g. [2, 3]). With respect to imaging of cancer, CEST has been shown to provide information of high clinical relevance spanning the diagnosis of tumors [3, 4], tumor grading [4, 5], and the assessment of therapy response after radiation treatment [6]. CEST became an emerging interest in the field of breast cancer diagnosis, revealing endogenous CEST contrasts in breast tumors [7–10].

The use of glucose has been proposed as a new molecular imaging approach for diagnosing tumors given its high sensitivity at the molecular level and the known enhanced glucose uptake by tumors [11]. However, its fast conversion to lactic acid prevents its efficient imaging. Several excipients and glucose analogs were tested as tumor-detecting agents in murine tumor models to assess their potential for clinical translation of CEST MRI [12]. Glucosamine (2-amino-2-deoxy-D-glucose, GlcN) is a glucose analog commonly used food supplement and has excellent safety profile. It is taken up by tumor cells through the glucose transporter, then undergoes phosphorylation and can accumulate in the cells [13, 14]. Recently, it was demonstrated as an exogenous contrast agent for imaging of breast tumors and their metastases in mice [15, 16]. Here, the translation of the GlcN CEST MRI method to a clinical MRI setup was examined, in order to evaluate the feasibility of obtaining a new class of contrast agent for breast cancer MRI that enables the tumor to be distinguished from the surrounding tissue, and to compare it to the conventional MRI method.

Material and methods

Subjects This study was reviewed and approved by the institutional review board (Tel Aviv and University and Sheba Medical Center); all patients signed informed consent. Twelve female patients with newly diagnosed breast lesions suspected as malignant cancer were included in this study, between August 2019 and March 2020. The histopathological markers of all enrolled patients are shown in Table 1. The patients were fasted for at least 6 h before the study and were scanned twice with the CEST MRI protocol: before and at 2 h after drinking a solution of 7.5 g of GlcN sulfate (Arthryl, Rafa) in 150 ml water.

MRI protocol All MRI measurements were performed on a 3-T clinical MRI scanner (PRISMA, Siemens) using a bilateral diagnostic breast coil (16 channels, Siemens) with the parameters listed in Supplementary Material (Table 1S). All acquisition parameters were optimized according to phantoms results of GlcN solutions at 3T [17]. The routine breast MRI protocol also included T_1W-DCE with the injection of gadoterate dimeglumine at a dose of 0.1 mmol/kg (Dotarem, Guerbet) contrast agent following the CEST scans.

Optimal slice positioning of the CEST sequence was supported by high-resolution T_2W images acquired at the beginning of the examination and unilateral shimming was performed to improve B_0 homogeneity. The CEST protocol included a series of saturation frequencies offsets (17–24) in the range of ± 6 ppm, using a train of 5 gauss saturation pulses with 100 ms long, interpulse delay of 61 ms and 2 s pause between measurements (total saturation pulse duration of 1.5–2 s), saturation attenuations of 2.5 μT, and recovery time of 5 s. One fully relaxed image was acquired for normalization. CEST sequence was applied with fat suppression and followed by a spiral-reordered 3D GRE read-out, resulting in a scan time of ~ 4–4.5 min.

Post processing Data processing was performed with Matlab 2017a (The Mathworks). Conventional Z-spectra were corrected for B_0 inhomogeneity (based on the B_0 field-maps [18]) and normalized. ROIs of the tumors and surrounding tissues were carefully selected by the radiologist who had originally read the case clinically and based on complementary data obtained by Gd-T_1W examinations. The calculation of the Z-spectra was performed on a voxel-by-voxel basis using spline interpolation of offsets acquired in the experiments [19]. Reported CEST values were averaged (mean ± standard deviation) within the defined ROIs based on magnetization transfer asymmetry (MTRasym) calculations:

$$CEST(\Omega) = [M_{SAT}(\Omega) - M_{SAT}(-\Omega)]/M_0 \quad (1)$$

where $M_{SAT}(\Omega)$ and $M_{SAT}(-\Omega)$ are the signal intensity with RF saturation at Ω and $-\Omega$, respectively, and M_0 is the signal intensity without RF saturation.

To resolve individual contributions to the GlcN CEST effect, the Z-spectrum was analyzed using a five-pool Gaussian

Table 1 Histological characteristics of the patients

Patient (no.)	Age (y)	Clips	Histologic type/grade	Phenotype ER/PR/ Her2	Necrosis	ACR breast	Ki-67 (%)
1	34	Yes	IDC, DCIS	+/+/+	No	B	20–25
2	50	Yes	IDC, DCIS/G3	+/+/	Yes	D	40
3	63	No	IDC/G3	+/+/+	No	C	30
4	43	No	DCIS	+/+/	No	D	-
5	75	No	IDC	+/+/+	No	B	20
6	38	No	IDC/G2+ DCIS low grade	+/+/-	No	C	5
7	46	No	IDC/G1	+/+/-	No	C	10
8	54	Yes	IDC/G2	+/+/+	No	C	30
9	50	Yes	IDC, low grade	+/+/-	No	C	-
10	68	Yes	IDC/G3 + extensive necrosis	-/-/-	Yes	B–C	95
11	50	Yes	IDC/G2–3	+/+/-	Yes	C	40
12	64	Yes	IDC/intermediate	+/-/+	No	C	-

Abbreviations: *IDC*, invasive ductal carcinoma; *DCIS*, ductal carcinoma in situ; *ER/PR/Her2*, estrogen/progesterone/Her2; *G1, G2, G3*, grade 1, 2, 3; *Ki67*, proliferation index (%). Tumor size was in the range of ~ 0.3–2 diameter

fitting model [20, 21] for the separation of the water, MT, hydroxyl, amine/amide, and NOE signals. Fitting the results by Gaussian functions was found to give better coefficient of determination (R^2) than the conventional Lorentzian fitting. The reason may be that field inhomogeneity had non-negligible contribution to the line shape. The fitting of the Z-spectrum to the sum of multiple Gaussian functions was performed using the following equation:

$$y = \sum_i A_i \exp\left[-41n2(x-\omega_i)^2/\sigma_i{}^2\right] \quad (2)$$

where ω is the frequency offset from the water resonance, and A_i, ω_i, and σ_i are the amplitude, frequency offset, and linewidth of the CEST peak for the i^{th} proton pool, respectively. The integrals of the different pools were generated following their multi-Gaussian fitting and are given as integral $= \sqrt{(\pi/2)}A_i\sigma_i$.

Contrast to noise ratio (CNR) was calculated as $(S_B-S_A)/\sqrt{(\sigma^2{}_B+\sigma^2{}_A)}$, where S_A and S_B are the mean values for the regions-of-interest (ROIs) of the tumors and the surrounding areas of normal breast tissue respectively and $\sigma_{A,B}$ are their standard deviations [22, 23]. In the same way, CNR was calculated for the T_1W imaging.

Statistical analysis The nonparametric Wilcoxon signed-rank test was used to calculate statistical significance as obtained before and after GlcN oral administration. p-values < 0.05 were considered significant. The small size of the study group does not allow the evaluation of the statistical significance of this research results vs. the clinical results.

Results

CEST signal was found to be higher in malignant breast lesions than in surrounding breast tissue in all patients (median age, 53 years, $N = 12$, $p = 2.2$ E−03) (Table 2 and Figs. 1, 2). The CEST signal was calculated based on MTRasym for chemical shifts at 2 ppm from the water signal. The choice of this chemical shift was to allow isolation from the broad water signal. The CEST signal location was determined based on complementary data obtained by Gd-T_1W examinations and according to its visual location as identified by an expert radiologist. Before the GlcN oral administration, the average CEST value for the tumors was 4.71 ± 3.31% while that of the normal tissue was 0.43 ± 0.36%. The average CEST values 2 h after the GlcN oral administration were 8.12 ± 4.09% and 0.48 ± 0.52% in the tumor and the normal tissues respectively ($N = 12$, $p = 2.2$ E−03). Thus, the average CEST value in the tumor increased by 3.41 ± 0.79% following the GlcN oral administration while that of the normal tissue remained about the same.

Figure 3 outlines the spectral results of the breast tumor as displayed with Z-spectra for patient no. 2. A multi-pool Gaussian fitting approach was applied to account for the contribution of each metabolite. Figure 3 points to the increase in the hydroxyl (OH) and amine/amide CEST signals as well as in the NOE signal of breast cancer tissue as observed by the Z-spectra following GlcN oral administration, indicating GlcN uptake in the tumors.

Both the Gaussian fitting analysis and MTRasym analysis show GlcN CEST effects in patients with breast tumors;

Table 2 Summary of all patients results as obtained from MRI data

Patient (no.)	T_1 contrast kinetics wash in (mm^2/s)	T_1 contrast kinetics wash out (rate/s)	T_1 contrast kinetics time to peak (s)	CNR T_1	MTRasym (before), % (2 ppm)	MTRasym (after), % (2 ppm)	Delta MRTasym, % (2 ppm)	CNR CEST (before)	CNR CEST (after)	Integrals calculated by Gaussian fitting					
										OH		Amine/amide		NOE	
										Before (1.5–2 ppm)	After	Before (2.5–4 ppm)	After	Before ((−2.8)–(−3.5) ppm)	After
1	0.7	0	133	4.6	6.8 ± 0.9	11 ± 0.8	4.2 ± 0.8	6.7	9.7	0.12	0.17	0.31	0.38	0.44	0.67
2		-		5.5	2.1 ± 1.2	6.8 ± 0.8	4.7 ± 1.0	1.6	7.4	0.32	0.48	0.39	0.58	0.29	0.49
3	0.43	2	96	4.6	4.2 ± 0.2	9.6 ± 1.4	5.4 ± 0.4	1.8	6.1	0.28	0.83	0.54	1.48	0.57	1.63
4	2.4	30	76	3.9	0.5 ± 0.3	2.9 ± 0.4	2.5 ± 1.6	0.9	5.9	0.2	0.24	0.62	0.69	0.34	1.14
5	2.4	0	133	3.1	11.4 ± 0.4	12.2 ± 0.2	0.8 ± 0.3	23.6	32.3	0.16	0.5	1.6	1.38	0.3	0.46
6	1.6	-	144	5.5	8.8 ± 0.5	10.7 ± 0.4	1.9 ± 0.4	9.4	17.4	0.13	0.57	0.4	0.67	0.49	0.5
7	2.1	0	142	5.1	6.9 ± 1.3	17.3 ± 0.8	10.4 ± 1.1	3.7	14.2	0.2	0.45	0.05	0.35	0.1	0.8
8	1.8	4	133	2.4	1.2 ± 0.5	6.7 ± 0.6	5.5 ± 0.5	1.1	6.8	-	-	-	-	-	-
9	1.19	12	142	2	6.5 ± 0.4	8.1 ± 0.5	1.6 ± 0.4	13.3	14.4	0.47	0.51	0.05	0.29	1.3	1.04
10	0.62	0	81	4.1	0.8 ± 0.5	3.5 ± 0.8	2.6 ± 0.6	1.2	3.8	0.26	0.57	0.72	1.03	1.05	1.79
11	1.09	-	146	3.8	2.4 ± 0.2	3.3 ± 0.6	0.9 ± 0.4	5.9	3.6	0.05	0.45	1.22	1.61	1.24	1.47
12	1.07	0	138	6	5.0 ± 0.7	5.4 ± 0.4	0.4 ± 0.6	5.6	6.2	0.14	0.31	0.54	0.81	0.32	0.53
Average	1.40		124	4.2	4.7	8.1	3.4	6.2	10.7	0.21	0.46	0.59	0.84	0.59	0.96
SD	0.67		25.1	1.3	3.3	4.1	0.8	6.7	8.1	0.11	0.17	0.44	0.45	0.40	0.47

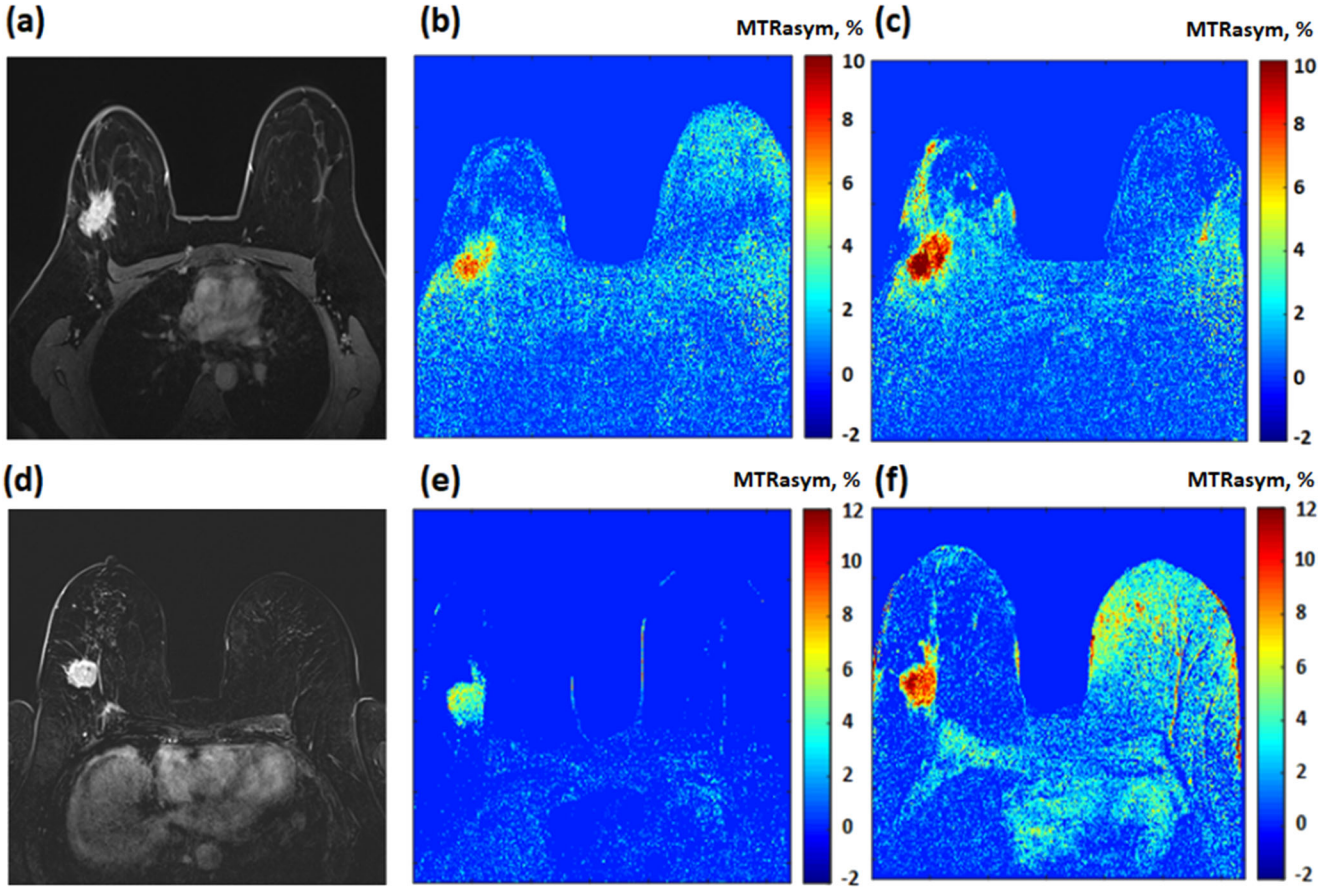

Fig. 1 **a–c** A 34-year-old female patient with grade II–III invasive ductal carcinoma in the right breast and (**d–f**) a 63-year-old female patient with grade III invasive ductal carcinoma in the right breast. **a**, **d** Gadolinium (Gd) T_1W images. **b**, **e** and **c**, **f** are CEST MTRasym maps calculated at frequency offset of 2 ppm before and after oral administration of GlcN, respectively

however, the Gaussian approach yields information of the different pool contributions to the Z-spectra as demonstrated in Fig. 4 and Table 2. Both CEST amplitudes and linewidths were increased after GlcN treatment (Table 2S, Supplementary Martial). The integrals for the hydroxyl, amine/amide CEST, and NOE pools were increased with averaged factors ($N = 12$) of 2.2 ± 1.2 (p = 3.38 E − 03), 1.4 ± 0.4 (p = 9.88 E − 03), and 1.6 ± 0.6 (p = 2.09 E − 02), respectively.

Discussion

To our knowledge, this is a first demonstration for the detection of human breast cancer with GlcN CEST MRI method at a clinical setup. This study reveals the feasibility of the technique to differentiate between breast cancer tissue and normal-appearing breast tissue. This observation suggests that the method could be used to track changes in metabolic activity in response to GlcN uptake in the tumor, a key marker for cancer diagnosis. Therefore, the method may be used as a complementary molecular imaging method. At the same time, determining the method's threshold conditions and thus identifying a typical GlcN CEST scale range for breast cancer will require a larger sample size. The high contrast to noise ratio (CNR) in the GlcN CEST images points to a potential in detecting small tumors at earlier stages. The MTRasym in the surrounding breast tissue was low, which is in agreement with recently published data [9].

This study showed that both the MTRasym analysis and the multi-pool Gaussian fitting may assist in detecting dynamic changes of the CEST signal in breast cancer following oral administration of GlcN. Since MTRasym calculations are impacted by the presence of other CEST species in the contralateral side of the direct effect, they were limited to the hydroxyl peak. Z-spectra were fitted with five Gaussian line shapes to separate the contributions of each peak contribution to the CEST effect. When compared with the results reported at higher preclinical field strength [16], lower absolute differences between the resonant frequencies of water and the other examined peaks at a clinical field strength give rise to considerably larger water direct saturation and spillover effects. In this study, we found that fitting to a Gaussian line shape [21] yielded better results than fitting to a Lorentzian line shape

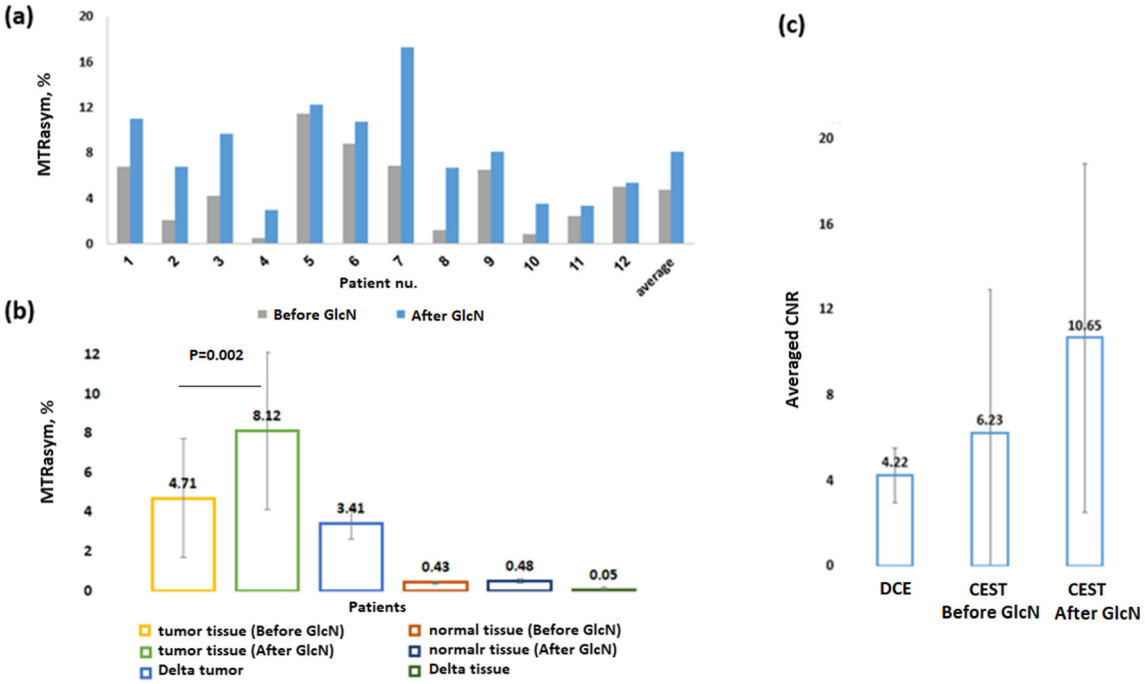

Fig. 2 Plots of the MTRasym at frequency of 2 ppm as obtained for tumor tissue measured in the patients (n = 12) (**a**) before and after oral administration of GlcN and (**b**) the average results compared with normal breast tissue (error bars represent the standard deviation of the distributions of MTRasym values) and (**c**) the averaged CNR results as obtained by the T_1W, and CEST imaging methods (error bars represent the standard deviation of the distributions of averaged CNR)

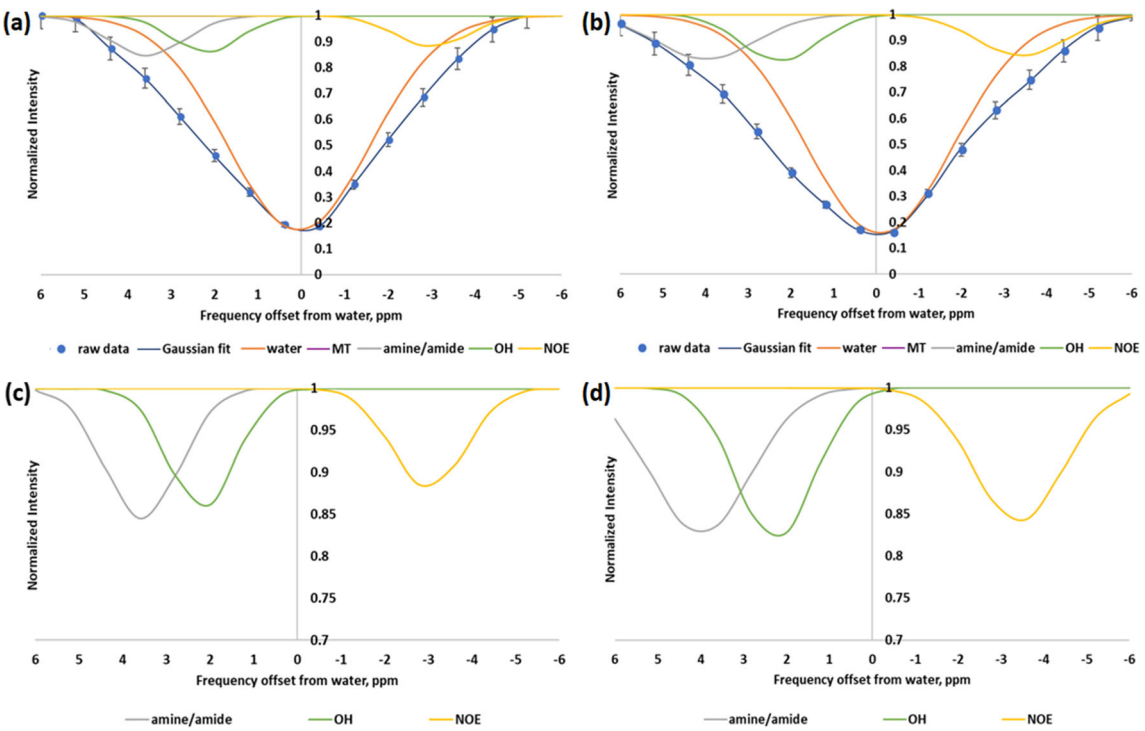

Fig. 3 Z-spectra of breast tumor obtained for a 50-year-old female patient with grade III IDC, DCIS in the left breast (**a**) before and (**b**) after oral administration of GlcN and the corresponding multi-pool Gaussian fitting, shows the contribution from different pools (error bars represent the standard deviation of the distributions of normalized intensities values). **c** and **d** are the fitted different pools, separated from the raw Z-spectra, respectively ($R^2 > 0.99$ and residual errors are less than 2%). The MT pool is not easily apparent in the figure since it is much smaller compared to the other pools

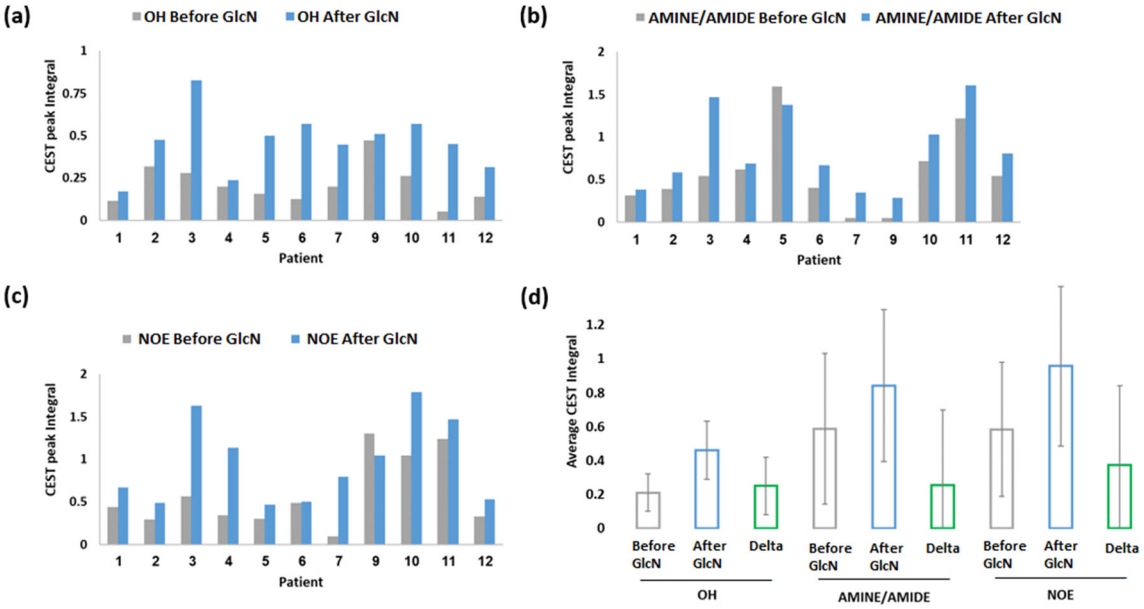

Fig. 4 CEST peak integral change for each examined patient at the frequency ranges of (**a**) OH, (**b**) amine/amide, and (**c**) NOE as calculated by the multi-pool Gaussian fitting before and after oral administration of GlcN and (**d**) the corresponding averaged CEST peak integral for the signals of the OH, amine/amide, and NOE (for all patients; patient #8 was excluded from the analysis due to technical difficulty in Z-spectra fitting)

[20]. This could be related to the fact that the 3-T clinical scanner contributes more to field inhomogeneity than the 7T results. The multi-Gaussian fitting approach allowed to measure tumor contrast referring to 3 main exchangeable pools: the hydroxyl, amine/amide, and NOE pools. The integral increase of the 3 peaks, which is attributed to GlcN administration, is due to an increase in both linewidth and amplitude of the examined pools. The contrast may arise from GlcN and its metabolic product accumulation in the tumor, as was previously shown for a murine model [15, 16]. Since there is limited published data regarding the metabolic activity of breast carcinomas, it is difficult to anticipate which type of exchangeable protons was detectable [7]. A CEST peak around 1.5–2 ppm may originate from –OH protons belonging to GlcN metabolites or from glycosaminoglycans (GAGs). The origin of the CEST contrast detected at 2.5–4 ppm may be a weighted sum of signals that originate from different amine/amide groups arising from GlcN and its phosphorylated products. As was shown previously [15], the CEST effect of GlcN increases at lower pH values. Hence, the enhanced CEST effect following the GlcN administration can also be explained by tissue acidosis associated with lactate buildup [16]. Potential contributions from metabolites responsible for the NOE (~−3 ppm) could be proteins and peptides as well as N-acetyl groups. The NOE effect indicates that the CEST arises from intracellular metabolites of GlcN. Free GlcN molecules do not give forth to NOE effects [15]. Thus, the observation of NOE proves that GlcN enters into the cancer cells and that its metabolites contribute to the CEST effect. This result concurs with previous ^{13}C NMR spectroscopy studies of extracts of implanted tumors in mice [16], which indicated the accumulation of GlcN and its metabolites in the tumors. One may note that the fat suppression has only a minimal effect on the CEST results since it is too short (few ms) to build up any additional CEST effects, and that this pulse is always applied even in the M_0 image; thus, a potential perturbation of the water will be offset independent.

The GlcN CEST contrast varies from patient to patient due to a variety of factors such as tumor viability and malignancy, pH change of the surrounding tissue, and individual reaction to GlcN administration, which might all contribute to the wide range of results. The small number of patients is a limitation of this study that may impede the ability to decide whether there is a significant correlation between the observed CEST results and pathological markers. Thus, further clinical trials are required to assess the detectability and the sensitivity of GlcN CEST signal with regard to the tumor pathological characteristics.

In the present study, each patient was scanned twice: before and 2 h after the administration of the agent. The choice of this time interval was done since it takes 2 h to get high concentration of GlcN in the blood [24]. This might be time constraints encountered in clinical practice. However, since GlcN CEST has highly significant contrast for breast tumors, it is reasonable to suggest that in the future a single scan (at a range of frequencies that are most sensitive for the detection of

GlcN) 2 h after oral administration of GlcN will be enough; thus, only an additional few minutes will be required over the routine clinical scan time.

In future, complementary studies should be performed in a larger scale of patients for further evaluation and optimization of the technique. Additionally, the GlcN CEST MRI technique should be examined for its ability to differentiate between malignant and non-malignant processes. In recent years, concerns have been raised regarding the repeated use of Gd [25]. GlcN CEST has potential clinical application that allows a non-Gd MRI of breast cancer. The similarity of the biochemical basis of the proposed method to that of the positron emission tomography (PET) points to the possibility that both morphological and metabolic information will be obtained in a single MRI session. It can serve as a guide for tumor diagnosis as well as its treatment monitoring.

Supplementary Information The online version contains supplementary material available at https://doi.org/10.1007/s00330-022-08772-w.

Acknowledgements We are indebted to the patients who participated in this research and we gratefully acknowledge Dr. Ilana Haas and Dr. Ravit Agassi for assisting in their recruitment.

Funding The authors gratefully acknowledge the support of this research by the Earlier.org - Friends For an Earlier Breast Cancer Test foundation and the Israel Science Foundation.

Declarations

Ethics approval Institutional Review Board approval was obtained.

Informed consent Written informed consent was obtained from all subjects (patients) in this study.

Conflict of interest The authors of this manuscript declare no relationships with any companies, whose products or services may be related to the subject matter of the article.

Guarantor The scientific guarantor of this publication is Prof. Gil Navon.

Statistics and biometry No complex statistical methods were necessary for this paper.

Methodology
- prospective
- diagnostic or prognostic study
- performed at one institution

References

1. Ward KM, Aletras AH, Balaban RS (2000) A new class of contrast agents for MRI based on proton chemical exchange dependent saturation transfer (CEST). J Magn Reson 143:79–87
2. Vinogradov E, Sherry AD, Lenkinski RE (2013) CEST: from basic principles to applications, challenges and opportunities. J Magn Reson 229:155–172
3. Wu B, Warnock G, Zaiss M et al (2016) An overview of CEST MRI for non-MR physicists. EJNMMI Phys 3:016–0155
4. Togao O, Yoshiura T, Keupp J et al (2014) Amide proton transfer imaging of adult diffuse gliomas: correlation with histopathological grades. Neuro Oncol 16:441–448
5. Takayama Y, Nishie A, Togao O et al (2018) Amide proton transfer MR imaging of endometrioid endometrial adenocarcinoma: association with histologic grade. Radiology 286:909–917
6. Meissner J-E, Korzowski A, Regnery S et al (2019) Early response assessment of glioma patients to definitive chemoradiotherapy using chemical exchange saturation transfer imaging at 7 T. J Magn Reson Imaging 50:1268–1277
7. Chan KW, Jiang L, Cheng M et al (2016) CEST-MRI detects metabolite levels altered by breast cancer cell aggressiveness and chemotherapy response. NMR Biomed 29:806–816
8. Krikken E, van der Kemp WJM, Khlebnikov V et al (2019) Contradiction between amide-CEST signal and pH in breast cancer explained with metabolic MRI. NMR Biomed 32:e4110
9. Zhang S, Seiler S, Wang X et al (2018) CEST-Dixon for human breast lesion characterization at 3 T: a preliminary study. Magn Reson Med 80:895–903
10. Klomp DWJ, Dula AN, Arlinghaus LR et al (2013) Amide proton transfer imaging of the human breast at 7T: development and reproducibility. NMR Biomed 26:1271–1277
11. Chan KWY, McMahon MT, Kato Y et al (2012) Natural D-glucose as a biodegradable MRI contrast agent for detecting cancer. Magn Reson Med 68:1764–1773
12. Longo DL, Moustaghfir FZ, Zerbo A et al (2017) EXCI-CEST: exploiting pharmaceutical excipients as MRI-CEST contrast agents for tumor imaging. Intern J Pharma 525:275–281
13. Anderson JW, Nicolosi RJ, Borzelleca JF (2005) Glucosamine effects in humans: a review of effects on glucose metabolism, side effects, safety considerations and efficacy. Food Chem Toxicol 43:187–201
14. Barron CC, Bilan PJ, Tsakiridis T, Tsiani E (2016) Facilitative glucose transporters: implications for cancer detection, prognosis and treatment. Metabolism 65:124–139
15. Rivlin M, Navon G (2016) Glucosamine and N-acetyl glucosamine as new CEST MRI agents for molecular imaging of tumors. Sci Rep 6:32648–32648
16. Rivlin M, Navon G (2021) Molecular imaging of cancer by glucosamine chemical exchange saturation transfer MRI: a preclinical study. NMR Biomed 34:e4431
17. Rivlin M, Barazany D, Navon G (2018) Chemical exchange saturation transfer (CEST) MRI of glucosamine at 3T. Proc Intl Soc Mag Reson Med 26:2275
18. Poblador Rodriguez E, Moser P, Dymerska B et al (2019) A comparison of static and dynamic ΔB(0) mapping methods for correction of CEST MRI in the presence of temporal B(0) field variations. Magn Reson Med 82:633–646
19. Stancanello J, Terreno E, Castelli DD, Cabella C, Uggeri F, Aime S (2008) Development and validation of a smoothing-splines-based correction method for improving the analysis of CEST-MR images. Contrast Media Mol Imaging 3:136–149
20. Zaiss M, Schmitt B, Bachert P (2011) Quantitative separation of CEST effect from magnetization transfer and spillover effects by Lorentzian-line-fit analysis of z-spectra. J Magn Reson 211:149–155
21. Zhang L, Zhao Y, Chen Y et al (2019) Voxel-wise Optimization of Pseudo Voigt Profile (VOPVP) for Z-spectra fitting in chemical exchange saturation transfer (CEST) MRI. Quant Imaging Med Surg 9(10):1714–1730

22. Rivlin M, Navon G (2018) CEST MRI of 3-O-methyl-D-glucose on different breast cancer models. Magn Reson Med 79:1061–1069
23. Zhou IY, Wang E, Cheung JS, Zhang X, Fulci G, Sun PZ (2017) Quantitative chemical exchange saturation transfer (CEST) MRI of glioma using Image Downsampling Expedited Adaptive Least-squares (IDEAL) fitting. Sci Rep 7:017–00167
24. Jackson CG, Plaas AH, Sandy JD et al (2010) The human pharmacokinetics of oral ingestion of glucosamine and chondroitin sulfate taken separately or in combination. Osteoarthritis Cartilage 18:297–302
25. Sherry AD, Caravan P, Lenkinski RE (2009) Primer on gadolinium chemistry. J Magn Reson Imaging 30:1240–1248